Buoyancy Assisted Janus Membrane Preparation by ZnO Interfacial Deposition for Water Pollution Treatment and Self#cleaning

Buoyancy Assisted Janus Membrane Preparation by ZnO Interfacial Deposition for Water Pollution Treatment and Self-cleaning

Tian-Di Pan, Zong-Jie Li, Da-Hua Shou, Wan Shou, Jin-Tu Fan, Xuqing Liu*, and Yong Liu**

Tian-Di Pan, Zong-Jie Li, Yong Liu

State Key Laboratory of Separation Membranes and membrane Processes

School of Textile science and engineering

Tianjin Polytechnic University

Tianjin 300387, China

E-mail: liuyong@tjpu.edu.cn

Da-Hua Shou, Jin-Tu Fan

Institute of Textiles and Clothing

The Hong Kong Polytechnic University

Hung Hom, Hong Kong, China

Wan Shou

Computer Science and Artificial Intelligence Lab (CSAIL)

Electrical Engineering and Computer Science Department

This is the author manuscript accepted for publication and has undergone full peer review but has not been through the copyediting, typesetting, pagination and proofreading process, which may lead to differences between this version and the Version of Record. Please cite this article as doi: 10.1002/admi.201901130.

Massachusetts Institute of Technology Cambridge

MA 02139, USA

E-mail: wanshou@mit.edu

Xuqing Liu

School of Materials

University of Manchester

Oxford Road, Manchester M13 9PL

E-mail: xuqing.liu@manchester.ac.uk

Water pollution, such as marine oil spill and organic chemicals pollution, is a worldwide challenge. To advance this emerging field, Janus membranes with asymmetric wettability, for oil-water separation, similitude of diode in electrocircuit, were fabricated by leveraging the buoyancy of Polyvinylidene fluoride (PVDF) nanofiber on water/air interface. ZnO nanowires are in situ grown on the surface of nanofibers immersed in the solution, mimicking a nanoscale Setaria viridis structure. Such Janus membrane showed a good hydrophilicity/underwater oleophobicity on ZnO nanowires modified side and exhibited opposite hydrophobicity on the other side. Due to the side-specific morphologies, this membrane can work either as "water-removing" type or "oil-removing" type filter as a diode in fluid. The membrane shows excellent permeability with the water and oil flux up to 1210 L m^{-2} h^{-1} and 7653 L m^{-2} h^{-1}, respectively, only driven by gravity. The durability of functional membrane is excellent, and separation efficiency is higher than 97.24% after 10 cycling tests. Furthermore, the hydrophilic side demonstrated an excellent photocatalytic performance over the degradation of rhodamine B dye, as self-cleaning properties. This Janus membrane is to be an excellent candidate for wastewater remediation, both oil/water separation and organic pollutant decomposition.

1. Introduction

The increasing oily wastewater, produced by food industries, metal/steel industries, textiles and the oil spill accidents, has become a global environmental problem.[] The oily wastewater brings many harmful chemicals with it, thus, threatens every specie including human being.[5-7] To deal with this issue, a variety of techniques including skimming, coagulation-flocculation, centrifugation, and membrane technology, have been reported so far.[8-9] Among these methods, membrane technology has been considered as an excellent candidate due to its high-efficiency and environmental friendly characteristics.[9]

It is well known that the separation of oil and water is mainly determined by surface energy (or wettability) of solid.[10] The surface geometry and chemistry are the critical factors, which determine the surface energy and wettability.[11] In general, there are two major kinds of materials for oil/water separation, hydrophobic/oleophilic material so-called “oil-removing” type and superhydrophilic/underwater superoleophobic material so-called “water-removing” type.[12] Recently, smart switchable materials have been intensively explored in the application of oil/water separation. Such surfaces can response to the stimulus to change wettability, including thermal treatment,[13-14] pH,[15] specific ion,[16-17]and light irradiation.[18]

However, such versatility limits their wide applicability and lacks reliability. Meanwhile, an external stimulus is required to realize the switch of wettability.[19] Therefore, for wide industrial and daily life applications, a straightforward, scalable, economical, and reliable separation technique is needed with switchable wettability. Namely, it should be a separator that can work for both water-removing (WR) as well as oil-removing (OR).[20]

Among various structural materials, the three-dimension (3D) nanomaterials due to their large surface area, high porosity and interconnected network,[21] have shown excellent capability in oil/water separation.[22-24] Herein, we report a facile strategy, inspired by natural plant (Setaria viridis), for the construction of 3D hybrid nanocomposite membrane with ZnO nanowires on PVDF nanofiber. PVDF nanofiber membrane was chosen for synthesizing the fluid diode owing to its high hydrophobicity,[25] which allows oil to pass while blocking water. Additionally, to impart the property allowing water transport while repelling oil, one side of the membrane was decorated with randomly oriented ZnO nanowires. Different from previous reports,[26-28] such ZnO nanowires with sharp tips are superhydrophilic and underwater oleophobic. If an addition interface, e.g., ZnO nanowires, was introduced on the surface of

PVDF nanofiber membrane, it would exhibited asymmetric properties on each side.[29] Thus ZnO@PVDF hybrid membrane would show a good hydrophilicity on ZnO nanowires side and hydrophobicity on the other side. By constructing such a Janus structure, the nanocomposite membrane gained the selectivity for oil/water separation, namely, the diodicity.[30] Furthermore, excellent photocatalytic performance was observed for ZnO@PVDF Janus membrane, as a self-cleaning property in oil/water separation.

2. Results and Discussion

The schematic demonstration of the fabrication process of ZnO@PVDF Janus membrane is illustrated in **Figure 1**a. The fabrication process initiated with the electrospinning of PVDF nanofibers (embedded with $Zn(Ac)_2$ as the precursor for ZnO seeds) followed by hydrothermal process to generate ZnO nanowires. Such fabrication method can be easily scaled up for industrial production, a digital photo of about 10 cm size membrane is displayed in **Figure 1b-iv**. The surface morphology of the ZnO@PVDF Janus membrane, characterized by scanning electron microscopy (SEM), shows Janus structure with nanowires protruding on the surface of nanofibers (**Figure 1bii-iii**), mimicking the Setaria viridis structure (**Figure 1b-i**).

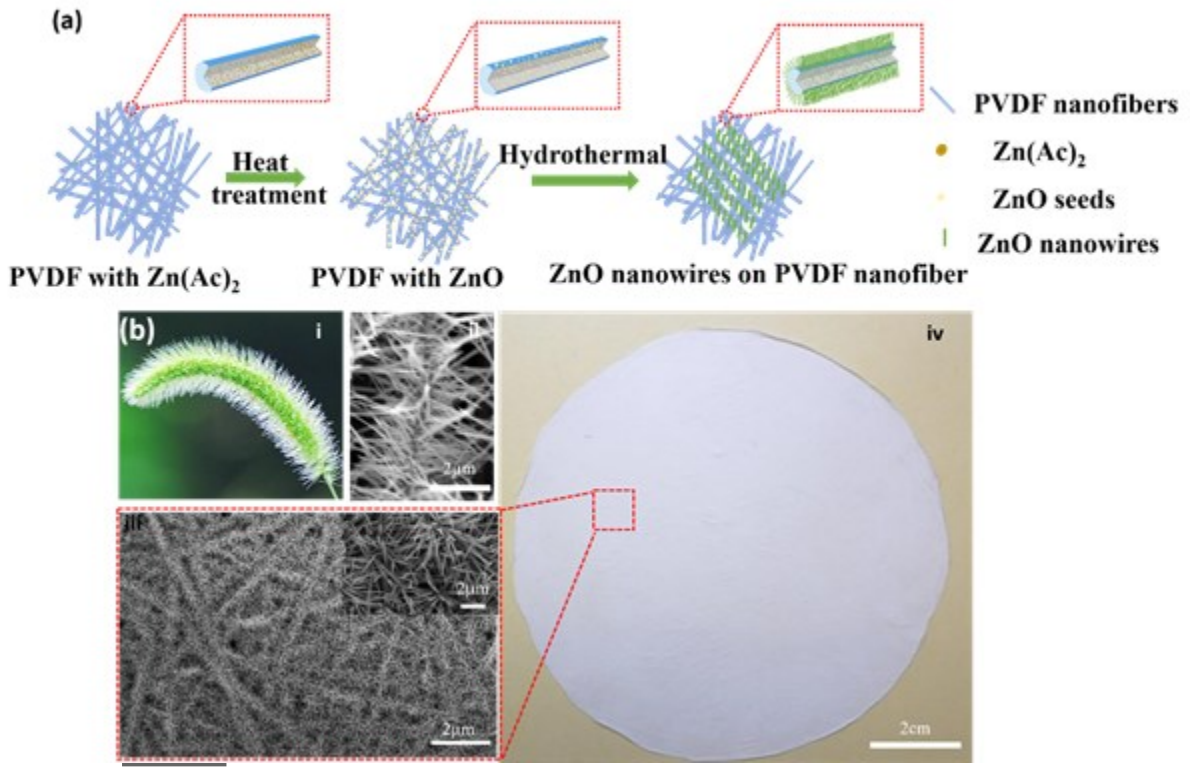

Figure 1. The biomimetic ZnO@PVDF Janus membrane with nanowires on nanofibers. (a) Procedure for the preparation of ZnO@PVDF Janus membrane. (b) i. Photo of Setaria viridis; ii. Illustration of nanowires on nanofiber; iii. SEM images of ZnO nanowires on PVDF nanofibers (inset: nanowires); iv. Photo of fabricated ZnO@PVDF Janus membrane.

For the comprehensive analysis of ZnO seed precursor influence on the morphology of electrospun nanofiber and the corresponding Janus membrane, SEM images of the membrane

obtained from different PVDF/$Zn(Ac)_2$ solutions were captured. The SEM images of ZnO@PVDF Janus membrane was shown in **Figure 2**. As shown in **Figure 2i**, PVDF/ZnO nanofibers presented a randomly distributed bead free porous membrane, with fiber diameter ranging from 150 to 700 nm. It was observed that the average nanofiber diameter decreased slightly with the increasing $Zn(Ac)_2$ content, which led to increased conductivity of the PVDF/$Zn(Ac)_2$ solutions (**Table s1**, supporting information). The higher conductivity of the electrospinning solution generated higher charge density on the surface of polymer jet increasing the jet acceleration towards grounded collector. This enhanced acceleration of polymer jet resulted into decreased fiber diameter of the resultant nanofibers.[31] **Figure 2** (the second row-ii) shows the SEM image of top side of ZnO@PVDF Janus membrane. It was noticed that the ZnO nanowires grew uniformly and radially along the randomly arranged nanofibers, mimicking a nanoscale Setaria viridis structure. It was noticed that when the $Zn(Ac)_2$ content was 0.5 wt%, membranes were not fully covered by ZnO nanowires (**Figure 2a-ii**). Also, in this case, the outline of nanofiber was not obvious, due to the long nanowires. With the increase of $Zn(Ac)_2$ content, the grown ZnO nanowires became shorter and denser, meanwhile, the shape of nanofiber became clear. The whole membrane was covered with random ZnO nanowires when the $Zn(Ac)_2$ content increases to 1.5 wt%. Such change is closely related to the number of ZnO seeds: with low $Zn(Ac)_2$ content (less ZnO seeds), each nucleation site can obtain sufficient Zn^{2+} source to grow longer nanowire. However, higher content of $Zn(Ac)_2$ (means more ZnO seeds) provided more nucleation sites for ZnO nanowire to grow, due to the competition between different nucleation sites, subsequent nanowires were relatively shorter. The SEM image of cross section of ZnO@PVDF Janus membrane was shown in Figure 2d-f. It is obvious that ZnO nanowires only grown on one side of the membrane (**Figure 2d**), which was immersed into the liquid during hydrothermal process. There was no ZnO nanowires on the other side of the membrane (**Figure 2e**).

Figure 2f provided the entire cross section of ZnO@PVDF Janus membrane, suggesting such Janus membrane were successfully prepared.

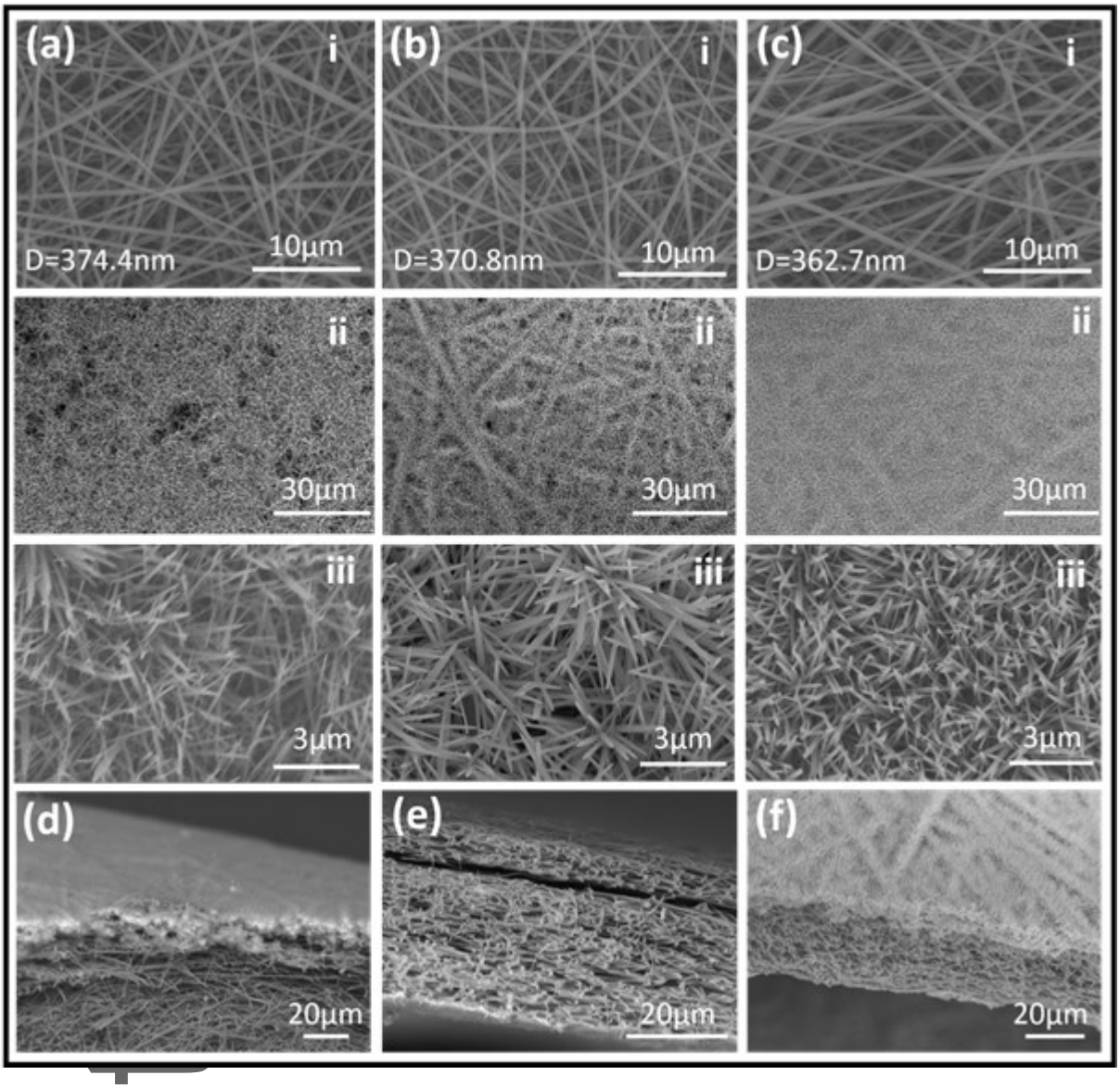

Figure 2. (a-c) SEM images of different sides of ZnO@PVDF Janus membrane made from different $Zn(Ac)_2$ concentration: (a) 0.5 wt%, (b) 1 wt% and (c) 1.5 wt%; i- the side of membrane without ZnO nanowires, and ii, iii- the side of membrane with ZnO nanowires . (d-f) SEM images of cross section of ZnO@PVDF Janus membrane.

To further elucidate the ZnO nanowire growth process, a comparative analysis via Fourier-transform infrared (FT-IR) spectroscopy of synthesized nanofiber membrane before and after thermal treatment was carried (**Figure 3**a). The major characteristic peaks at 840, 878, 1072, 1168, 1280 and 1401 cm^{-1} representing the β-phase of PVDF,[32] are present in both as electrospun nanofibers and heat-treated ones, indicating the existence of PVDF. However, the peak at 1582 cm^{-1} corresponding to the carboxylate group disappeared after heat treatment at 130 ˚C, which indicates the decomposition of $Zn(Ac)_2$ and conversion to ZnO seeds during heat treatment.[33] The ZnO seeds facilitated the growth of ZnO nanowires by providing nucleation sites during the hydrothermal growth process.[34] The X-ray diffraction (XRD) spectra of PVDF/ZnO nanofiber membrane and hybrid nanocomposite membranes are shown in **Figure 3b**. In the PVDF/ZnO nanofiber membrane curve, the peak at 21.1˚ was attributed to the β phase (110) of PVDF,[35] which is consistent with the FT-IR results. Whereas, the peak at 36.6˚ was related to the (101) plane of ZnO which confirmed the formation of ZnO seeds during the heat treatment. The XRD diffractogram of hybrid nanocomposite membrane shows the presence of additional peaks at 2θ=31.6˚ (100), 34.3˚ (002), 36.1˚ (101), which correspond to the hexagonal wurtzite structure. The

presence of zinc nitrate hydroxide was witnessed by 2θ=24.9° (400).[36] The narrow, sharp diffraction peaks suggested ZnO nanowires are highly crystalline. These results demonstrate that the ZnO nanowires were successfully immobilized on the surface of PVDF nanofibers. Based on the above analysis, the formation of ZnO nanowires in the low temperature hydrothermal reaction can be explained using the following chemical reaction Equations. First, the dissolution of zinc nitrate generated zinc ions (Equation (1)). Then, hexamethylenetetramine (HMTA), a pH buffer solution, slowly released OH^- ions (Equation (2) and (3)). Then, the zinc oxide nanowires grew at the low supersaturation of the reactants (Equation (4)).[37]

$$Zn(NO_3)_2 \rightarrow Zn^{2+}+2(NO_3)^- \quad (1)$$

$$C_6H_{12}N_4+6H_2O \rightarrow 6HCHO+4NH_3 \quad (2)$$

$$NH_3+H_2O \rightarrow NH_4^+ +OH^- \quad (3)$$

$$Zn^{2+}+2(OH)^- \rightarrow Zn(OH)_2 \rightarrow ZnO+H_2O \quad (4)$$

Structural characterization of the pristine and resultant ZnO@PVDF Janus membrane was carried out using nitrogen adsorption-desorption analyzer (**Figure S1**, supporting information). With the introduction of ZnO nanowire, there was a significant increase in the specific surface area of the resultant hybrid membrane (15.18 m^2/g) compared to the pristine PVDF membrane (7.18 m^2/g). Thermal performance of the pristine and ZnO@PVDF Janus membranes was examined by a thermogravimetric analyzer (TGA) in air atmosphere. It was found that the membrane had a

endothermic peak at 258 ˚C, which was associated with water removal of zinc nitrate hydroxide.[38] Both PVDF membrane and ZnO@PVDF Janus membrane showed similar degradation profiles. However, the two regions in ZnO@PVDF Janus membrane showed a shift to lower temperature due to the presence of ZnO (**Figure 3c**). Compared with PVDF membrane, the largest degradation temperature (where the DTG showed the largest value) of ZnO@PVDF Janus membrane decreased by 5 and 53 ˚C. The presence of metal Zn seems activate the decomposition of PVDF. Similar results were reported by Cacho-Bailo on the addition of MOF in polysulfone.[39] Therefore, the thermal stability of ZnO@PVDF Janus membrane decreased. In addition, ZnO@PVDF Janus membrane offered excellent mechanical characteristics (**Figure 3d**). High tensile strength of ZnO@PVDF Janus membrane (7.18 MPa) compared to pristine PVDF membrane (3.49 MPa) indicates the mechanical robustness of ZnO@PVDF Janus membrane. The enhanced mechanical properties were attributed to the decreased fiber diameter due to the addition of $Zn(Ac)_2$, the formation of inter-fiber bonding and the enhanced crystallinity of PVDF nanofibers due to heat treatment.[40] Furthermore, the incorporation of ZnO nanowires improved the stiffness while decreasing the ductility.

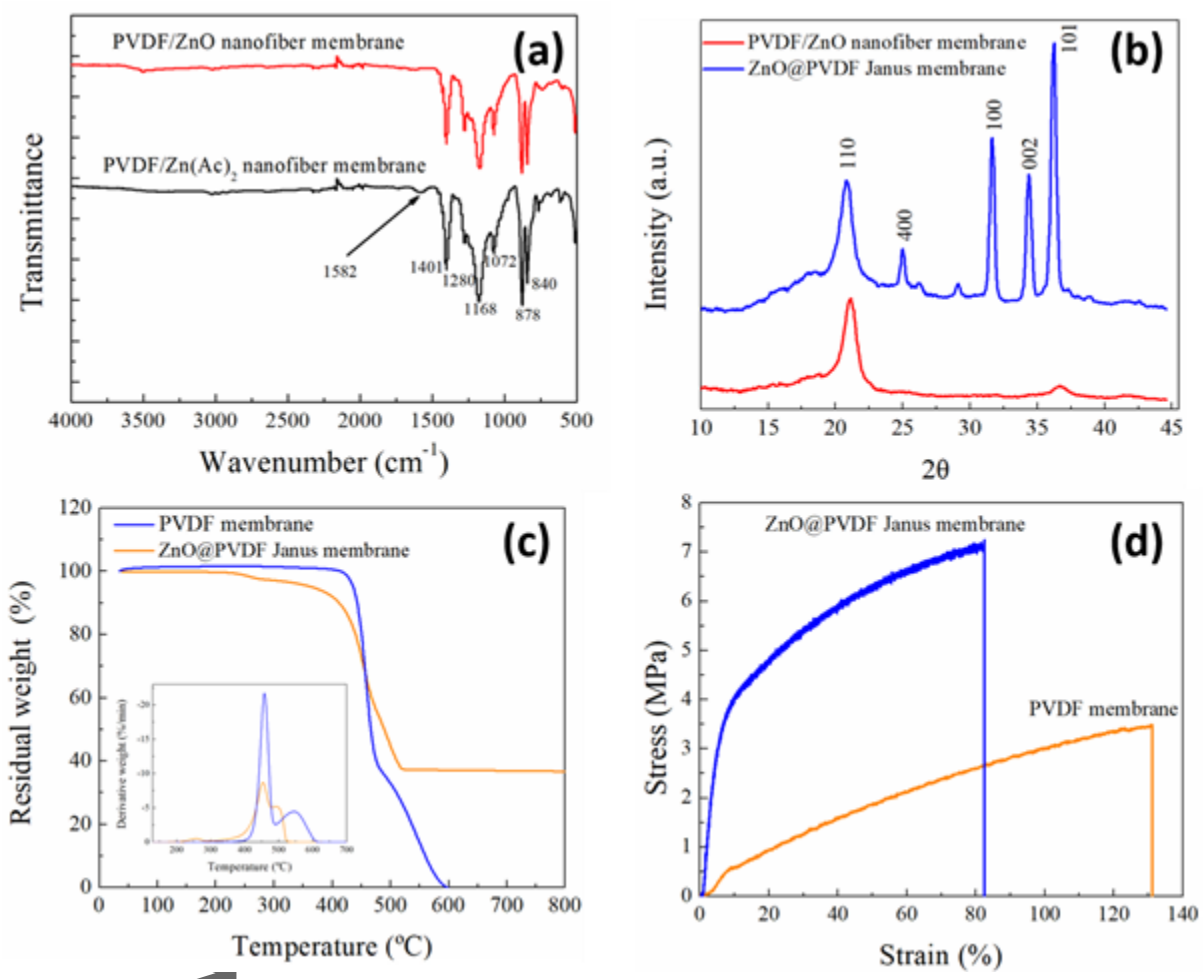

Figure 3. (a) FTIR spectra of nanofibers membrane before and after heat treatment; (b) XRD patterns of nanofibers membrane before and after hydrothermal growth of ZnO; (c) TGA curves of PVDF membrane and ZnO@PVDF Janus membrane (inset: corresponding DTG curves); (d) Stress-strain curves of PVDF and ZnO@PVDF Janus membrane.

In order to validate the applicability of this ZnO@PVDF Janus membrane as a fluid diode for oil/water separation, the wettability was examined first. **Figure 4**a shows the water contact angle (CA) behaviour on the top side of ZnO@PVDF Janus membrane of different

weight ratios of $Zn(Ac)_2$ concentration. With the increase of $Zn(Ac)_2$ concentration, the water CA decreased from 127° to 11°. This change in wettability of inherently hydrophobic PVDF nanofibers was credited ZnO nanowires which caused the change in surface morphology. The conical structure of ZnO nanowires led to a Laplace pressure (ΔP) between tip and base of ZnO nanowires,[41] which is expressed as

$$\Delta P=\int_{R_2}^{R_1} \frac{2\gamma}{(R+R_0)^2} \sin\alpha dz \quad (5)$$

where R, R_1 and R_2 are the local radius of cones, R_0 is the radius of water droplet, γ is the surface tension of water, α is the half-apex angle of cone, and dz represents the increasement radius of the cone. Such driving force made the water droplet move from the tip to base side along ZnO nanowires. On the other hand, the wettability of solid surface is associated with the roughness and chemical compositions, the growth of ZnO nanowires not only increased the roughness but also introduced massive hydroxyl groups.[42] The roughness can be described by Wenzel's Equation as follow:[43]

$$\cos\theta_w = r \cdot \cos\theta \quad (6)$$

where r indicates the surface roughness factor defined as the ratio of actual surface area to the geometric surface area, θ_w and θ represent the apparent and intrinsic contact angles. From Equation (6), the value of $\cos\theta_w$ increased according to the surface roughness increase. Generally, the apparent contact angle decreased when the material was hydrophilic. The AFM images of the surface of PVDF membrane and ZnO@PVDF Janus membrane were shown in **Figure S2**. The surface roughness of ZnO@PVDF Janus membrane (2.06 nm) was higher than that of PVDF membrane (0.02 nm), which was obviously attributed to ZnO nanowires grown on PVDF nanofibers. As shown in **Figure 4b**, the water contact angle (CA) of the bottom side of ZnO@PVDF Janus membrane was 134±3° (with pH~7), indicating the good hydrophobicity. Additionally, ZnO@PVDF Janus membrane exhibited robust hydrophobicity towards the water with a broad range of pH (1-7, **Figure 4b**), demonstrating excellent stability and usability. Further increase of the pH from 8 to 11, the CA decreased to ~110°, which was attributed to probable defluorination and introduction of hydroxyl and carbonyl groups.[44] On contrary, the top side of the membrane shows superhydrophilicity and underwater oleophobicity with CA of 140±3° at pH~7. (**Figure 4c**, also see **Movie S1** and **S2**).

Robust oleophobicity was maintained with pH from 1 to 7, but the CA of oil droplet in water decreased to ~110˚ as well, with pH value increased to 11, which is attributed to the reaction with basic solution (or dissolution), and subsequent surface morphology change.[45-46] Thus, ZnO@PVDF Janus membrane presented different wettability on each side, i.e. superhydrophilicity and hydrophobicity, as shown in **Movie S3**.

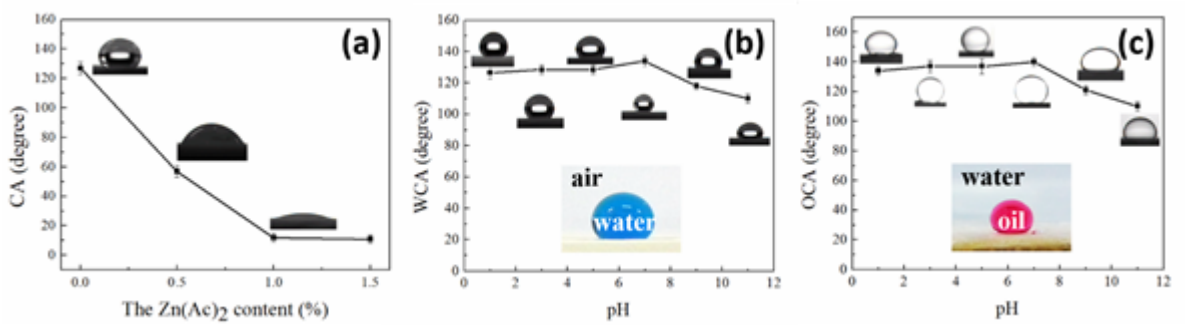

Figure 4. (a) The influence of $Zn(Ac)_2$ content on the water contact angle of ZnO@PVDF Janus membrane (top side); (b) The relationship between the pH and the water contact angles of ZnO@PVDF Janus membrane (bottom side); (c) The relationship between the pH and the underwater oil contact angles of ZnO@PVDF Janus membrane (top side). All tests were performed at 25 ˚C.

To further demonstrate the membranes' application as fluid diode for oil/water mixture separation, n-hexane, cyclohexane, petroleum ether, soybean oil and CCl_4 were taken as representative oils. **Figure 5**a show forces acting on the water or oil droplets of membrane.

When separating light oil/water mixture, assuming the downward as plus direction, the force for water or oil droplet was described as follows:

$$F_w = H_p + G_w + F_c - f \quad (7)$$

$$F_o = H_p + G_o - f_o \quad (8)$$

where F_w is the force for water droplet in light oil/water mixture, H_p is the hydrostatic pressure due to the force of gravity,[47] G_w is the gravity of water droplet, F_c is the capillary force given to the water droplet in the hydrophilic side, f is adhesive resistance, F_o is the force for oil droplet in light oil/water mixture, G_o is the gravity of oil droplet, f_o is the buoyancy for light oil droplet (**Figure 5a-i**). In contract, separating heavy oil/water mixture, the force for water or oil droplet was described as follows:

$$F'_w = H'_p + G'_w - f'_w \quad (9)$$

$$F'_o = H'_p + G'_o + F'_c - f' \quad (10)$$

where F'_w is the force for water droplet in heavy oil/water mixture, H'_p is the hydrostatic pressure due to the force of gravity, G'_w is the gravity of water droplet, f'_w is the buoyancy for water droplet, F'_o is the force for oil droplet in heavy oil/water mixture, G'_o is the gravity of oil droplet, F'_c is the capillary

force given to the oil droplet in the hydrophobic side, f' is adhesive resistance (**Figure 5a-ii**). It can be deduced that $F_w > 0$ and $F'_o > 0$, which realized selective oil/water separation. For the separation of oils lighter than water, the top side of ZnO@PVDF Janus membrane was wetted by water beforehand and the only driving force was gravity. When the mixture of petroleum ether and water (dyed with the methylene blue) at a weight ratio of 1:2 was poured into the separation device, water permeated through the membrane and dropped into the beaker, while the petroleum ether remained in the glass apparatus (**Figure 5b-i** and **Movie S4**). Additionally, ZnO@PVDF Janus membrane shows a water flux of 1210 L m^{-2} h^{-1}. For the separation of oils heavier than water, the bottom side of ZnO@PVDF Janus membrane was used without any treatment. When the mixture of water and CCl_4 (dyed with the oil red) was poured into separation device, CCl_4 quickly passed through ZnO@PVDF Janus membrane and dropped into the beaker, whereas the water remained in the glass apparatus (**Figure 5b-ii**, and **Movie S5**). ZnO@PVDF Janus membrane exhibited a permeation flux of CCl_4 about 7563 L m^{-2} h^{-1}. This flux is much higher than that of water, which should be attributed to its lower viscosity ($\eta_{CCl_4}=0.969 mPa \cdot s$) compared with that of water ($\eta_{H_2O}=1 mPa \cdot s$) and the hydrophobic/superoleophilic property of PVDF.[9, 48-49] The permeate flux and separation performance vary with oil/water mixtures, as shown in **Figure 5c**. Overall, ZnO@PVDF Janus membrane exhibited excellent separation efficiency from 98.33% to 99.84%, as well as high water flux, which is close or even better than most modified commercial PVDF membrane.[50-51] The relatively lower separation efficiency of water/CCl_4 mixture may be associated with their volatility.[52] In addition, all the separation efficiency maintained at above 97% of water or heavy oil after 10 cycles of testing as shown in **Figure 5d**. Thus, ZnO@PVDF Janus membrane is a

promising candidate for separating oil/water mixtures, which can be employed on demand for either water-removing or oil-removing separation.

FIGURE 5.TIF

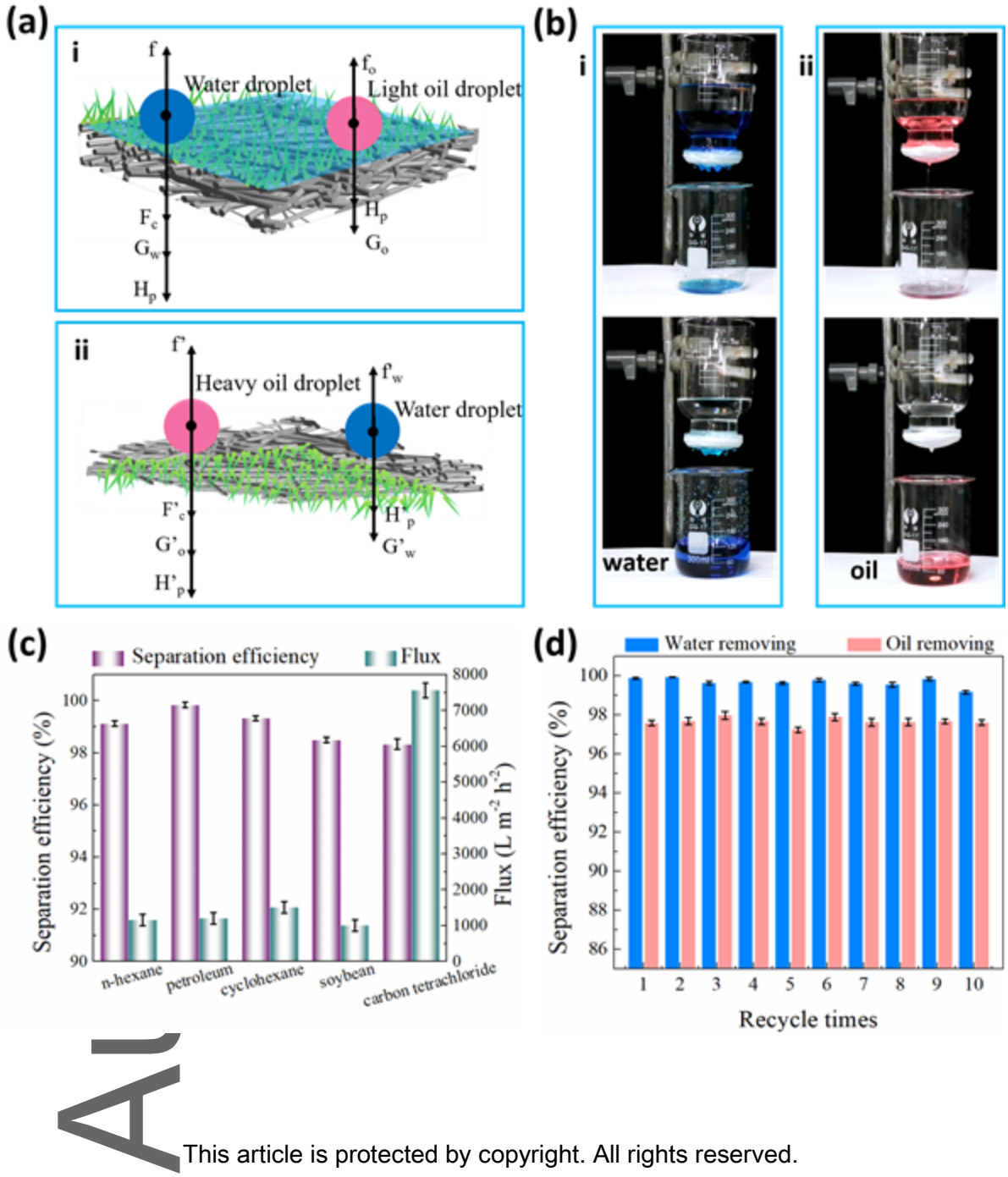

Figure 5. The oil/water separation experiment and results. (a) Force diagrams of droplets on ZnO@PVDF Janus membrane: (i)force diagram of water and oil droplet on the hydrophilic side when pre-wetted with water. (ii) force diagram of water and oil droplet on the hydrophobic side (b) Photo of oil/water separation setup: (i) $\rho_{oil} < \rho_{water}$, water (dyed with the methylene blue) permeates through membrane, while the oil remained in the glass apparatus (petroleum ether); (ii) $\rho_{oil} > \rho_{water}$, CCl_4 (dyed with the oil red) quickly passes through the membrane, while the water remained in the glass apparatus; (c) The separation efficiency and flux of ZnO@PVDF Janus membrane for different oils. (d) Cycling performance of ZnO@PVDF Janus membrane. All tests were performed at 25 ˚C.

Lastly, the photocatalytic degradation performance of ZnO@PVDF Janus membrane was evaluated using Rhodamine B (RhB) under UV irradiation, to show the ability of decomposing chemical pollutants in water, as well as the self-cleaning performance. As shown in **Figure 6**a, the intensity of characteristic absorption peak of RhB at 554 nm significantly decreased with the increase of time. Meanwhile, a blue shift could be observed, which was caused by the N-deethylation of RhB.[53] The colour of RhB changed from pink to colourless which may be to cleavage of the chromophoric groups.[54] Afer the conjugated structure of RhB was destructed, ring opening and mineralization occurred, which converted to carbon dioxide and water.[55-56] Compared with the self-degradation of RhB, no obvious change was observed for the PVDF membrane case as indicated

in **Figure 6b**. After 1 h UV irradiation, ZnO@PVDF Janus membrane degraded nearly 73.25% of RhB, while the self-degradation of RhB was 5.72%. The degradation efficiency of ZnO@PVDF Janus membrane was 98.93% after 2 h exposure, which is comparable to previous studies.[42, 57-58] After five cycles, the degradation efficiency of ZnO@PVDF Janus membrane remained about 95% (**Figure 6c**) and there was no noticeable change of the membrane surface with ZnO nanowires (**Figure S3**). The results show that ZnO@PVDF Janus membrane have excellent photocatalytic activity and photocatalytic stability. With further optimization, the functional ZnO@PVDF Janus membrane can realize oil/water separation and dye removal simultaneously.

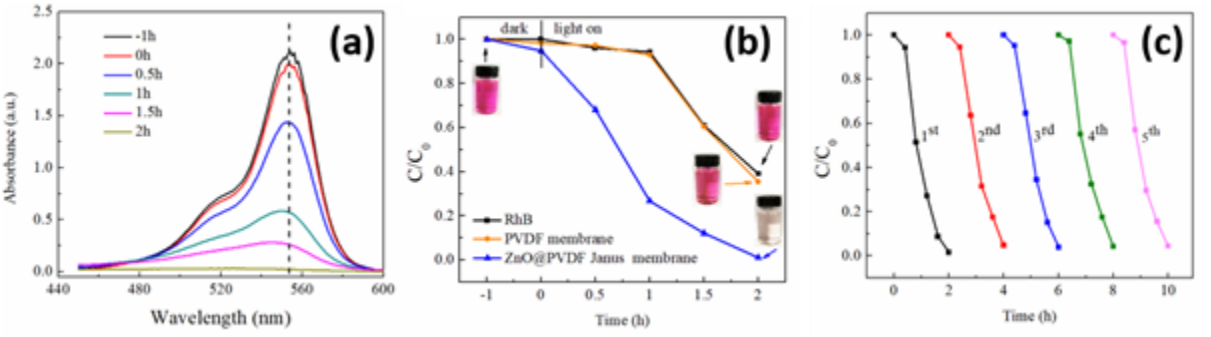

Figure 6. (a) UV-vis absorbance spectra of RhB as a function of time over ZnO@PVDF Janus membrane under UV illumination; (b) The photocatalytic degradation efficiency of RhB in the presence of ZnO@PVDF Janus membrane; (c) cycling tests of ZnO@PVDF Janus membrane under UV irradiation. All the photocatalytic reaction temperature were controlled at 20 ˚C.

3. Conclusions

In summary, a Janus membrane with 3D hybrid nanostructures was successfully fabricated with electrospinning method and hydrothermal growth. This membrane exhibited a

superhydrophilicity/underwater oleophobicity on ZnO nanowires side and presented hydrophobicity on the other side, which can work as a high-performance fluid diode for oil/water separation. By simply switching the side of a membrane, it can work for water removing as well as an oil-removing filter only driven by gravity. The synthesized membrane also showed decent mechanical and chemical stability. With whole separation efficiency more than 97.24%, this Janus membrane also showed good recyclability. Furthermore, designed membrane exhibited excellent photocatalytic activity and photocatalytic stability, and maintained the degradation efficiency of RhB of nearly 95% under UV irradiation after five cycles, showed excellent self-cleaning property. Finally, this present study provides a scalable strategy for functional fluid diode fabrication which can be used for highly efficient oil/water separation and waste-water remediation.

4. Experimental Section

Materials: PVDF (Mw=517,000) was purchased from Solvay. Zinc acetate dihydrate ($Zn(Ac)_2$), zinc nitrate hexahydrate(ZNH) and hexamethylenetetramine (HMTA) were supplied by Tianjin Fengchuan Chemical Reagent Technology Co., Ltd. N,N-dimethylformamide (DMF), acetone, n-hexane, cyclohexane, petroleum ether, soybean

oil and carbon tetrachloride(CCl_4), dichloromethane(CH_2Cl_2) were obtain from Tianjin Kermel Co., Ltd., China. Methylene blue was obtained from Sinopharm Chemical Reagent Co., Ltd., China. Rhodamine B (RhB) was purchased from Meryer Chemical Technology Co., Ltd., China. All reagents were used without further purification.

Fabrication of PVDF/Zn (Ac)$_2$ nanofiber membranes: PVDF was dissolved in DMF and acetone solvent (w/w=3:1) at a concentration of 17%. $Zn(Ac)_2$ was added into the solution of PVDF to form a spinning solution. The $Zn(Ac)_2$ concentrations were 0.5, 1.0 and 1.5 wt%, respectively. The PVDF/$Zn(Ac)_2$ solution was stirred magnetically at 90 ˚C for 6 h. After that, the PVDF/$Zn(Ac)_2$ solution was loaded into syringes. The syringe needles were positively charged with 10 kV. The feed rate was maintained at 0.5 ml h^{-1}. The distance between the syringe needle tips and the collector was 16 cm.

Preparation of ZnO@PVDF Janus membranes: The PVDF/$Zn(Ac)_2$ nanofibers membranes were subjected to heat treatment at the temperature of 130 ˚C for 24 h to obtain ZnO seeds. The obtained PVDF/ZnO nanofibers membranes were treated for 3 h in ZNH and HMTA aqueous solution of 0.01 mol L^{-1} at 95 ˚C in an oven. This hydrothermal reaction led to the formation of ZnO@PVDF Janus membrane with ZnO nanowires on PVDF nanofiber. The preparation process of ZnO@PVDF Janus membrane is shown in **Figure 1a**. During the hydrothermal reaction, ZnO nanowires were selectively grown on one side of PVDF membrane by making use of buoyancy, leaving only one side in contact with the solution.

Characterizations: The morphology of membranes was studied by electron microscopy (FE-SEM S-4800, and SEM TM3030, Hitachi, Japan). Before observation, the membranes

were sputtered with gold. The structural information of membranes was measured by Fourier transform infrared spectroscopy (FT-IR, TENSOR37, Germany). The crystallization patterns of ZnO particles and nanowires were determined by X-ray diffraction (XRD, D8 Discover, USA). Thermal stability of membranes was analyzed with thermalgravimetric analysis instrument (TG, NETZSCH, Germany) under air atmosphere at a heating of 10 ˚C min^{-1} in the temperature range of 25-800 ˚C. The mechanical properties were measured with a tensile testing machine (Instron 3369, USA) under a load cell of 5 kN and the tensile speed was 10 mm min^{-1}, the clamping distance was 20 mm, the samples were cut into 10×40 mm^2. The Brunauer-Emmett-Teller specific surface area of membranes was measured using nitrogen adsorption-desorption analyzer (Autosorb-iQ-C, Quantachrome, USA). Water or oil contact angle (CA) was recorded by a Contact Angle Measuring Instrument (JYSP-180, China). Five different positions were measured under the same sample and the average CA was obtained. The surface roughness of membrane was measured with atomic force microscopy (AFM, Bruker, USA). The test area was 3x3$\boldsymbol{\mu m^2}$.

Oil/water separation tests: ZnO@PVDF Janus membrane was fixed on the bottle of filter cup (diameter is 39 mm), with a beaker placed under the filter cup. For the separation of oils lighter than water, the top side of ZnO@PVDF Janus membrane was placed upward, which was wetted by water beforehand and the only driving force was gravity. When 180 g of light oil/water mixture (water dyed with the methylene blue) at a 1:2 weight ratio was poured into separation device, water permeates through the membrane and drops into the beaker, while the petroleum ether remained in the filter cup. For the separation of oils heavier than

water, the bottle side of ZnO@PVDF Janus membrane was placed upward, which was directly fixed on the bottle of filter cup. When 180 g of heavy oil/water mixture (oil dyed with the oil red) at a 2:1 weight ratio was poured into separation device, heavy oil quickly passes through the membrane and drops into the beaker, whereas the water remained in the filter cup. The separation efficiency η was calculated by the following Equation:

$$\eta = \frac{m_1}{m_0} \times 100$$

where m_1 is the weight of the penetration component, m_0 is the initial weight of the penetration component.

Photocatalytic degradation measurement: The photocatalytic activity of ZnO@PVDF Janus membrane was evaluated by the decomposition of RhB (10 mg L^{-1}) in water. First, a mixture of 3×3 cm^2 of hybrid nanocomposite membrane photocatalyst and 20 mL of RhB solution were placed in a 50 mL beaker in the dark for 1 h to reach the absorbance-desorbance equilibrium. Then the beakers were transferred to a photo-reactor at controlled temperature (20 ˚C), under high pressure mercury lamp irradiation (CEL-LAM500, Beijing Aulight Technology Co., Ltd, 500 W, with a maximal emission at 365 nm). The distance between the RhB solution surface and the lamp tube was 15 cm. Finally, the beaker was taken out at intervals of 0.5 h. The concentrations of RhB were measured by UV-vis spectrophotometer (ThermoFisher Scientific, USA) with the maximum absorbance of 554 nm. The degradation efficiency was calculated by using the following Equation:

$$degradation(\%)=(C_0-C)/C_0 \times 100$$

where C_0 is the initial concentration of RhB and C is the RhB concentration after irradiation.

Supporting Information

Supporting Information is available from the Wiley Online Library or from the author.

Acknowledgements

T. P. and Z. L. contributed equally to this work. The authors gratefully acknowledge financial support by the National Natural Science Foundation of China (Grant No. 51573133), the China Postdoctoral Science Foundation Grant (2018M630276) and Natural Science Foundation of Ningbo (No. 2018A610104).

Conflict of Interest

The authors declare no conflict of interest.

Received: ((will be filled in by the editorial staff))
Revised: ((will be filled in by the editorial staff))
Published online: ((will be filled in by the editorial staff))

Reference

[1] A. K. Kota, G. Kwon, W. Choi, J. M. Mabry, A. Tuteja, Nat. Commun. **2012**, *3*, 1025.

[2] P. C. Chen, Z. K. Xu, Sci. Rep. **2013**, *3*, 2776.

[3] F. Zhang, W. B. Zhang, Z. Shi, D. Wang, J. Jin, L. Jiang, Adv. Mater. **2013**, *25*, 4192.

[4] J. Zhang, S. Seeger, Adv. Funct. Mater. **2015**, *21*, 4699.

[5] M. A. Shannon, P. W. Bohn, M. Elimelech, J. G. Georgiadis, B. J. Mariñas, A. M. Mayes, Nature **2008**, *452*, 301.

[6] Q. Ma, H. Cheng, Y. Yu, H. Ying, Q. Lu, S. Han, J. Chen, W. Rong, A. G. Fane, Z. Hua, Small **2017**, *13*, 1700391.

[7] Q. Ma, Y. Yu, M. Sindoro, A. G. Fane, R. Wang, H. Zhang, Adv. Mater. **2017**, *29*, 1605361.

[8] C. Lee, S. Baik, Carbon **2010**, *48*, 2192.

[9] S. Xiong, L. Kong, J. Huang, X. Chen, Y. Wang, J. Membrane. Sci. **2015**, *493*, 478.

[10] D. Tian, X. Zhang, X. Wang, J. Zhai, L. Jiang, Phys. Chem. Chem. Phys. **2011**, *13*, 14606.

[11] B. Wang, W. Liang, Z. Guo, W. Liu, Chem. Soc. Rev. **2015**, *44*, 336.

[12] Z. Xue, S. Wang, L. Lin, L. Chen, M. Liu, L. Feng, L. Jiang, Adv. Mater. **2011**, *23*, 4270.

[13] B. Xue, L. Gao, Y. Hou, Z. Liu, L. Jiang, Adv. Mater. **2013**, *25*, 273.

[14] Z. Xu, Y. Zhao, H. Wang, H. Zhou, C. Qin, X. Wang, T. Lin, Acs Appl. Mater. Inter. **2016**, *8*, 5661.

[15] B. Cheng, Z. Li, Q. Li, J. Ju, W. Kang, M. Naebe, J. Membrane. Sci. **2017**, *534*, 1.

[16] Z. Liu, W. Wang, R. Xie, X.-J. Ju, L.-Y. Chu, Chem. Soc. Rev. **2016**, *45*, 460.

[17] Z. Liu, X.-J. Ju, Y.-H. Huang, R. Xie, W. Wang, K.-R. Lee, L.-Y. Chu, J. Membrane. Sci. **2016**, *497*, 328.

[18] D. Tian, X. Zhang, Y. Tian, Y. Wu, X. Wang, J. Zhai, L. Jiang, J. Mater. Chem. **2012**, *22*, 19652.

[19] X. Yue, Z. Li, T. Zhang, D. Yang, F. Qiu, Chem. Eng. J. **2019**, *364*, 292.

[20] D. Ge, L. Yang, C. Wang, E. Lee, Y. Zhang, S. Yang, Chem. Commun. **2015**, *51*, 6149.

[21] F. R. Dina, Z. Adriana, B. Thomas, Chem. Rev. **2014**, *114*, 9487.

[22] X. Tang, Y. Si, J. Ge, B. Ding, L. Liu, G. Zheng, W. Luo, J. Yu, Nanoscale **2013**, *5*, 11657.

[23] J. Zhang, Z. Meng, J. Liu, C. Schlaich, Z. Yu, X. Deng, J. Mater. Chem. A **2017**, *5*, 16369.

[24] Y. Si, Q. Fu, X. Wang, J. Zhu, J. Yu, G. Sun, B. Ding, Acs Nano **2015**, *9*, 3791.

[25] Y. Liao, R. Wang, M. Tian, C. Qiu, A. G. Fane, J. Membrane. Sci. **2013**, *425-426*, 30.

[26] G. Kwak, M. Seol, Y. Tak, K. Yong, J. Phys. Chem. C **2009**, *113*, 12085.

[27]M. Gong, Z. Yang, X. Xu, D. Jasion, S. Mou, H. Zhang, Y. Long, S. Ren, J. Mater. Chem. A **2014**, *2*, 6180.

[28] U. P. Shaik, D. D. Purkayastha, M. G. Krishna, V. Madhurima, Appl. Surf. Sci. **2015**, *330*, 292.

[29] H. C. Yang, Y. Xie, J. Hou, A. K. Cheetham, V. Chen, S. B. Darling, Adv. Mater. **2018**, *30*, 1801495.

[30] J. E. Mates, T. M. Schutzius, J. Qin, D. E. Waldroup, C. M. Megaridis, Acs Appl. Mater. Inter. **2015**, *6*, 12837.

[31] X. Zong, K. Kim, D. Fang, S. Ran, B. S. Hsiao, B. Chu, Polymer **2002**, *43*, 4403.

[32] M. M. Abolhasani, K. Shirvanimoghaddam, M. Naebe, Compos. Sci. Technol. **2017**, *138*, 49.

[33] G. Xiong, U. Pal, J. G. Serrano, K. B. Ucer, R. T. Williams, Physica Status Solidi **2006**, *3*, 3577.

[34] Q. L. Huang, Y. Huang, C. F. Xiao, Y. W. You, C. X. Zhang, J. Membrane. Sci. **2017**, *534*, 73.

[35] T. Wu, B. Zhou, T. Zhu, J. Shi, Z. Xu, C. Hu, J. Wang, Rsc Adv. **2015**, *5*, 7880.

[36] G. Hua, L. Zhang, J. Dai, L. Hu, S. Dai, Appl. Phys. A **2011**, *102*, 275.

[37] B. Weintraub, Z. Zhou, Y. Li, Y. Deng, Nanoscale **2010**, *2*, 1573.

[38] G. G. C. Arizaga, J. E. F. da Costa Gardolinski, W. H. Schreiner, F. Wypych, J. Colloid Interf. Sci **2009**, *330*, 352.

[39] F. Cacho‐Bailo, C. Téllez, J. Coronas, Chem. Eur. J. **2016**, *22*, 9533.

[40] S. S. Choi, Y. S. Lee, W. J. Chang, S. G. Lee, J. K. Park, K. S. Han, Electrochim. Acta **2004**, *50*, 339.

[41] J. Ju, H. Bai, Y. Zheng, T. Zhao, R. Fang, L. Jiang, Nat. Commun. **2012**, *3*, 1247.

[42] X. Zhang, J. Qin, Y. Xue, P. Yu, B. Zhang, L. Wang, R. Liu, Sci. Rep. **2014**, *4*, 4596.

[43] R. N. Wenzel, Transactions of the Faraday Society **1936**, *28*, 988.

[44] G. J. Ross, J. F. Watts, M. P. Hill, P. Morrissey, Polymer **2000**, *41*, 1685.

[45] A. L. Chen, X. U. Dong, X. Y. Chen, W. Y. Zhang, X. H. Liu, T. Nonferr. Metal Soc. **2012**, *22*, 1513.

[46] X. Wang, Q. Zhang, Q. Wan, G. Dai, C. Zhou, B. Zou, J. Phys. Chem. C **2012**, *115*, 2769.

[47] W. Jing, N. Wang, W. Li, D. Hua, J. Lei, Soft Matter **2012**, *8*, 5996.

[48] W. Zhang, Z. Shi, F. Zhang, X. Liu, J. Jin, L. Jiang, Adv. Mater. **2013**, *25*, 2071.

[49] F. Yang, Y. Li, X. Yu, G. Wu, J. Yu, B. Ding, Rsc Adv. **2016**, *6*, 87820.

[50] H. Shi, Y. He, Y. Pan, H. Di, G. Zeng, L. Zhang, C. Zhang, J. Membrane. Sci. **2016**, *506*, 60.

[51] X. Yang, Y. He, G. Zeng, X. Chen, H. Shi, D. Qing, F. Li, Q. Chen, Chem. Eng. J. **2017**, *321*, 245.

[52] W. Bai, M. Guan, N. Lai, R. Yao, Y. Xu, J. Lin, Mater. Chem. Phys. **2018**, *216*, 230.

[53] S. Rasalingam, C.-M. Wu, R. T. Koodali, ACS Appl. Mater. Inter. **2015**, *7*, 4368.

[54] M. Sundararajan, V. Sailaja, L. J. Kennedy, J. J. Vijaya, Ceram. Int. **2017**, *43*, 540.

[55] X. Li, T. Wan, J. Qiu, H. Wei, F. Qin, Y. Wang, Y. Liao, Z. Huang, X. Tan, Appl. Catal. B: Environ. **2017**, *217*, 591.

[56] D. Xu, X. Sun, X. Zhao, L. Huang, Y. Qian, X. Tao, Q. Guo, Water, Air, Soil Poll. **2018**, *229*, 317.

[57] M. A. Alvi, A. A. Al-Ghamdi, M. Shaheerakhtar, Mater. Lett. **2017**, *204*, 12.

[58] E. Rokhsat, O. Akhavan, Appl. Surf. Sci. **2016**, *371*, 590.

Table of Contents

Buoyancy Assisted Janus Membrane Preparation By Zno Interfacial Deposition For Water Pollution Treatment

Tian-Di Pan, Zong-Jie Li, Da-Hua Shou, Letian Wang, Wan Shou, * Jin-Tu Fan, Xuqing Liu*, and Yong Liu*

Keyword: Janus membrane, ZnO Nanowires, Oil/water separation, Photocatalysis

ZnO@PVDF Janus membrane is fabricated by electrospinning and hydrothermal reaction. The fabricated membrane with ZnO nanowires on PVDF nanofiber showed a good hydrophilicity/underwater oleophobicity on ZnO nanowires side and exhibited hydrophobicity on the other side. The membrane provides a scalable strategy for functional fluid diode fabrication which can be used for high efficient oil/water separation.

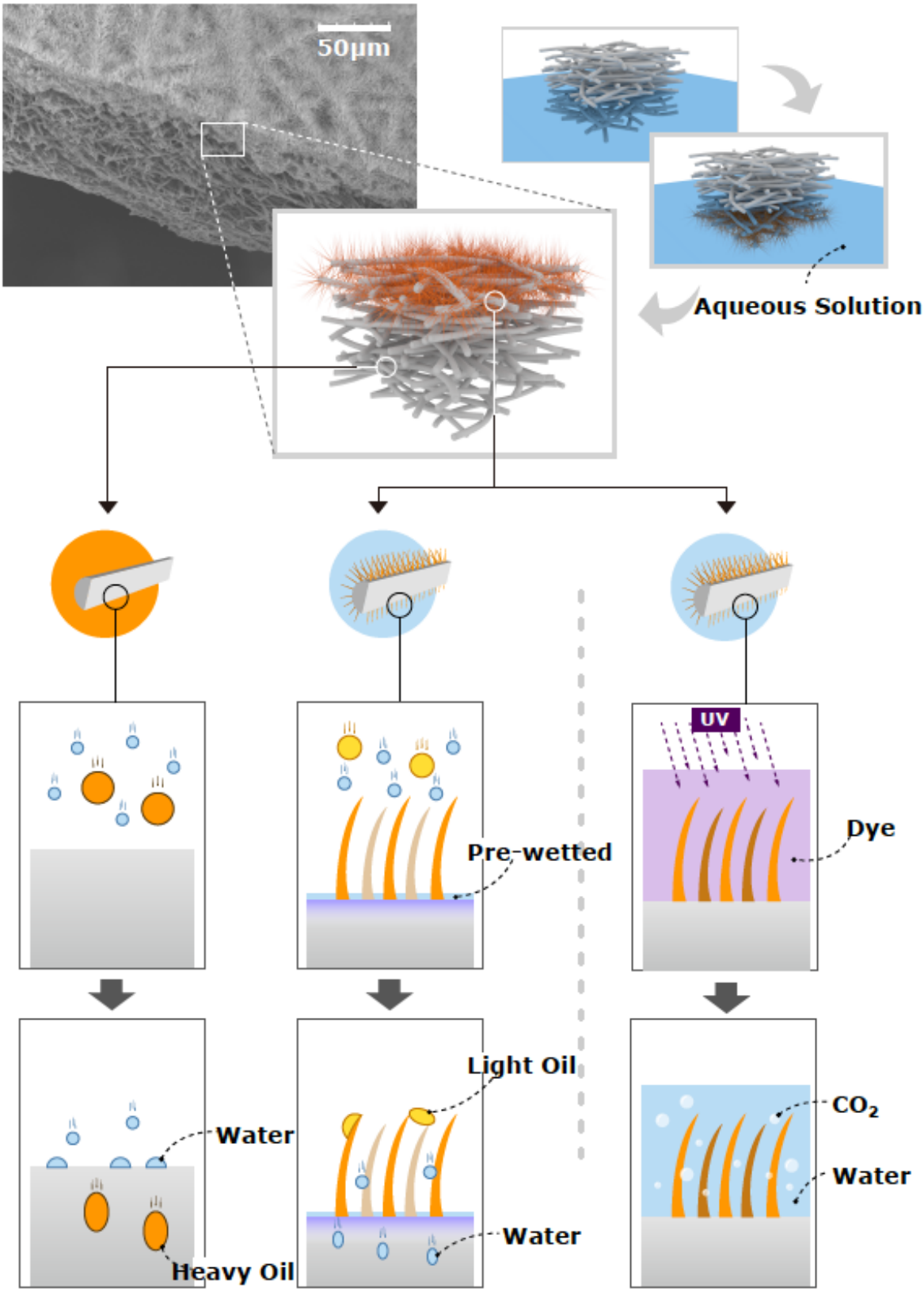
50μm
Aqueous Solution
UV
Pre-wetted
Dye
Water
Heavy Oil
Light Oil
Water
CO_2
Water